Nanoscale

Accepted Manuscript

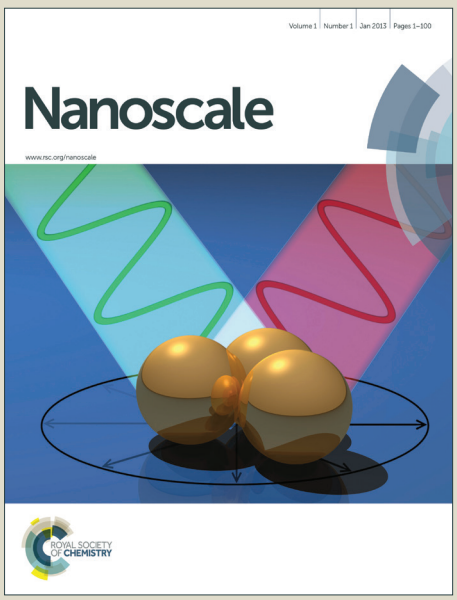

ROYAL SOCIETY OF CHEMISTRY

www.rsc.org/nanoscale

Nanoscale

ARTICLE

Cerium oxide nanoparticles, combining antioxidant and UV shielding properties, prevent UV-induced cell damage and mutagenesis

Received 00th January 20xx,
Accepted 00th January 20xx

DOI: 10.1039/x0xx00000x

www.rsc.org/

Fanny Caputo[a,b], Milena De Nicola[a,b], Andrej Sienkiewicz[c], Anna Giovanetti[d], Ignacio Bejarano[a,e], Silvia Licoccia[b], Enrico Traversa[b,e] and Lina Ghibelli[a,†]

The efficient inorganic UV shields, mostly based on refracting TiO_2 particles, dramatically changed sun exposure habits. Unfortunately, health concerns emerged from the pro-oxidant photocatalytic effect of UV-irradiated TiO_2, which mediates toxic effects on cells. Therefore, improvement of cosmetic solar shield technology is a strong priority. CeO_2 nanoparticles are UV refractors but also potent biological antioxidants due to surface 3+/4+ valence switch, which confers anti-inflammatory, anti-ageing and therapeutic properties. Here we set up UV irradiation protocols, allowing selectively studying the extra-shielding effects of CeO_2 vs. TiO_2 nanoparticles on reporter cells. TiO_2 irradiated with UV (especially UVA) exerted strong photocatalytic effect, superimposing their pro-oxidant, cell-damaging and mutagenic action to that induced by UV, thereby worsening UV toxicity. On the contrary irradiated CeO_2 nanoparticles, *via* their Ce^{3+}/Ce^{4+} redox couple, exerted impressive protection on UV-treated cells, buffering oxidation, preserving viability and proliferation, reducing DNA damage and accelerating repair; strikingly, they almost eliminated mutagenesis, proposing as important tools to prevent skin cancer. Interestingly, CeO_2 nanoparticles also protected cells from damage induced by irradiated TiO_2, suggesting that the two particles may complement their effects also in solar lotions. CeO_2 nanoparticles, intrinsically coupling UV shielding with biological and genetic protection, seem therefore ideal candidates for next-generation sun shields.

Introduction

The ultraviolet region of the electromagnetic spectrum includes wavelength falling in the A (400-315 nm), B (315-280 nm), and C (280-100 nm) categories[1]. UV rays deeply interact with living matter, behaving as biological regulators but also as stressors affecting cells and tissues. UVB and UVC directly damage DNA, causing genetic mutations and cancer[2]. Moreover, UV rays activate intracellular chromophores that generate reactive oxygen species (ROS), promoting oxidative stress, a condition responsible for many pathological states and ageing[3]. Cells damaged by UV that are not correctly repaired may lose viability and undergo cell death by apoptosis[4], or survive with genetic alterations and cause cancer[2]. The direct targets of UV damage are the skin and the eye[5], but also systemic effects of UV exposure have been described, including the imbalance of the inflammatory response[6].

Practices of leisure and professional exposure to sunlight have dramatically changed since the development and diffusion of UV-shielding lotions. Inorganic shields included in modern sun protection products are mostly based on titanium dioxide particles, in the form of needle-like or near spherical shape rutile and/or anatase nanocrystals[7,8], two crystal forms acting as stable and efficient UV-shields. The formulations containing nanosized particles allow obtaining transparent lotions and therefore nanosized TiO_2 is preferred by the cosmetic industry. For this

[a] Dipartimento di Biologia, Università di Roma Tor Vergata, Roma, Italy
[b] Dipartimento di Scienze e Tecnologie Chimiche; Università di Roma Tor Vergata, Roma, Italy;
[c] Institute of Physics of Complex Matter, Faculty of Basic Sciences, École Polytechnique Fédéral de Lausanne, Lausanne, Switzerland,
[d] UTBIORAD, ENEA, Roma, Italy,
[e] King Abdullah University of Science and Technology, Thuwal, Saudi Arabia.
† Correspondence to: ghibelli@uniroma2.it

reason the market of UV-shielding lotions containing nano-formulation of TiO_2 has dramatically increased in the last years[8]. However, concern for sunshield customers' health comes from the notion that anatase and rutile particles, including those present in commercial sunscreens, if irradiated with UV in aqueous environment[9-11], produce ROS via the photocatalytic effect[12] and enhance ultraviolet damage of DNA and cells in in vitro systems in spite of the shielding effect[7,8,13-18]. Therefore under sun exposure TiO_2, while blocking the UV radiation reducing direct UV damage, promote a secondary oxidative stress constituting a health hazard[19-21]. Strategies aimed to overcome this problem are presently a focus of great interest, focusing on the addition of molecular[22,23] or particulate [24] antioxidants. However, the results have been so far deceiving because of the instability of the antioxidants to the persistent solar irradiation.

Cerium oxide (CeO_2) are able to shield UV rays[25,26]. Thanks to their shielding activity, CeO_2 nanoparticles have been first proposed as an alternative to TiO_2 and ZnO_2 in sunscreen lotions by Yabe *et al.*[27-29]. Interestingly, it was recently shown[30] that a combination of TiO_2/CeO_2 nanoparticles allows better refractory properties, increasing the sun protection factor (SPF) provided by the TiO_2 nanoparticles formulations presently adopted in commercial lotions.

In addition to their shielding properties, CeO_2 nanoparticles act as potent antioxidants due to the redox switch of cerium ions in the 3+ and in the 4+ valence state in the oxide, as reviewed by different groups[31-35]. The Ce^{3+}/Ce^{4+} redox couple has been shown to exert robust antioxidant effects undergoing 3+ to 4+ transition when dismutating superoxides[31,32,36-38], and regenerating the reduced valence catalysing the transformation of H_2O_2 in H_2O + O_2 [32,36-38]. Thus, CeO_2 nanoparticles abate the most noxious ROS in a catalytic, energy-free and auto-regenerative fashion. Accordingly, CeO_2 nanoparticles protect cells[32,33,36,39-41] and animals[32,33,36,42,43] from many different insults, exert strong anti-apoptotic effects[31,44], ameliorating many serious oxidant-related pathologies[32,33,36,45,46] promoting wound healing[33]; moreover, CeO_2 nanoparticles exert potent and intriguing anticancer effects[47,48].

The coexistence of UV-refracting and anti-oxidant, cell protective effects of CeO_2 nanoparticles suggests that they may serve as multitasking tools to protect from risks related to exposure to sunlight, by shielding UV rays on one side, and protecting from the noxious effects of the residual radiation products on the other. Two pioneering works by Zholobak *et al.*[25,35] investigated the protective effect of CeO_2 nanoparticles on UV-irradiated epithelial cell lines, showing that a pre-treatment with CeO_2 nanoparticles significantly increases viability in UV-ray-irradiated cells. However, working with adherent cell models where nanoparticles necessarily form a shield over the cell monolayer, they were not able to discriminate between the physical shielding effects and the biological activity exerted by CeO_2 nanoparticles.

The main objective of this study is therefore to evaluate the extra-shielding effects of CeO_2 nanoparticles and analyse the mechanisms involved, and to establish a comparison with the effects exerted by TiO_2 nanoparticles. In addition, we wanted to investigate the eventual CeO_2 nanoparticles protective effects against the photocatalytic activity of TiO_2, to explore the possibility of using a mixture of the two particles in solar lotions, exploiting the higher UV-filtering ability of TiO_2 nanoparticles on one side, and the persistent, autoregenerative ability of CeO_2 nanoparticles on the other.

Results and discussion

Photocatalytic and UV-shielding properties of TiO_2 and CeO_2 nanoparticles

To obtain nanoparticles of similar size and shape, TiO_2[49,50] and CeO_2[31,50] nanoparticles were prepared according to wet chemical synthetic procedures, which allow tailoring the powder features[49-52]. These synthetic procedures are well established in our lab and very reproducible.

TiO_2 precursors were heated at 450°C, obtaining 10 nm single anatase phase nanoparticles (labelled as TiO_2) as shown by the XRD patterns (Figure 1A) selected area electron diffraction patterns (SAED) and the transmission electron microscopy (TEM) micrographs (Figure 1B). The heating temperature was selected according to the results of simultaneous thermogravimetric and differential thermal analysis (TG-DTA), which showed that at 400°C the weight loss ended in correspondence with the crystallization of the amorphous precursor in the anatase phase.

Cerium oxide nanoparticles (labelled here as CeO_2) of the same size were obtained by heating the CeO_2 nanoparticles precursor to 450°C, which was the same procedure that allowed optimizing the previously reported CeO_2 nanoparticles redox activity[31,51,53]. Also in this case the annealing temperature was selected according to the

TG-DTA results, which showed that at 450°C the sample was crystalline with a stable weight. The thermal treatment was necessary to eliminate all the organic residues, which may alter the native biological properties of CeO_2 nanoparticles, whose analysis is the scope of this study.

The $Ce^{3+/4+}$ redox switch that confers antioxidant activity to CeO_2 nanoparticles can be abolished by doping with Sm, which substitute for Ce^{3+} ions in the nanoparticle lattice[31]; Sm-doped CeO_2 nanoparticles has been exploited to investigate the role played by the 3+/4+ redox switch in CeO_2 nanoparticles catalytic activity[31], including the antioxidant bio-effects[31]. For this study, 20% Sm-doped CeO_2 nanoparticles (labelled as SDC) were synthesized as described by Esposito et al.[52] to obtain samples to significantly lower the Ce^{3+} concentration, while maintaining the content of oxygen vacancies with respect to the CeO_2 nanoparticles sample. As previously demonstrated by our group[31], increasing concentrations of Sm ions (5-20%) dose-dependently reduced the anti-oxidant activity of CeO_2 nanoparticles in abiotic as well as in biological systems, being totally abolished with 20% doping, concentration that was chosen for the present study.

Figure 1 reports the physico-chemical characterization of the different NPs tested. Figures 1A and 1B shows the XRD, the SAED and the TEM micrographs, respectively, for the CeO_2 and SDC nanoparticles samples. The particles are shown to be crystalline by XRD and SAED analysis. TiO_2 is shown to possess an anatase crystal structure, while CeO_2 and SDC nanoparticles are characterized by the fluorite crystal structure of cerium oxide. Particle size measured using transmission electron microscopy (TEM) observations was in the 5-16 nm range. The BET specific surface area was measured in the 57-47 m^2 g^-1 range, a value smaller than the theoretical expected, due to nanoparticles aggregation[31].

To measure the UV shielding efficiency of the three types of nanoparticles, the UV absorbance spectra were recorded in water media for the dispersions of the prepared samples, as shown in Figure 1C. The results obtained are in line with the values reported by other abiotic studies[25-28] showing high shielding efficiency of TiO_2 powder, good absorption in the UV region for CeO_2 nanoparticles, and a weaker effect for SDC nanoparticles.

Figure 1D summarizes the physico-chemical features of the three nanopowders and their colloidal dispersions properties in H_2O and in physiological media.

An XPS analysis was performed to measure the Ce^{3+}/Ce^{4+} ratio in CeO_2 vs. SDC nanoparticles as reported by Celardo et al.[31], showing a significant decrease in Ce^{3+} concentration (6% *vs.* 21%) by 20% Sm-doping. Zeta potential values measured in water at pH 7.4 are negative for all the NPs tested, being slightly lower for SDC NPs, probably due to a small increase in their size. Importantly, the zeta potential values measured in biological media become neutral for all the NPs tested (between -10 and 10 mV), due to the absorption of serum proteins. Therefore, we can exclude that the NPs tested may present a different biological behavior in cellular culture experiments due to differences in their surface charge.

We then analysed the photocatalytic effect of the three powders irradiated with visible light, UVA, UVB or UVC by EPR analysis using α-(4-Pyridyl N-oxide)-N-tert-butylnitrone POBN as a spin trap. Figure 2 shows that anatase produce a strong EPR signal after UVA, UVB and UVC irradiation, whereas CeO_2 nanoparticles are ineffective, confirming previous results[26]. The EPR signal of TiO_2 is compatible with production of hydroxyl radical, which is very reactive and dangerous in biological environments.

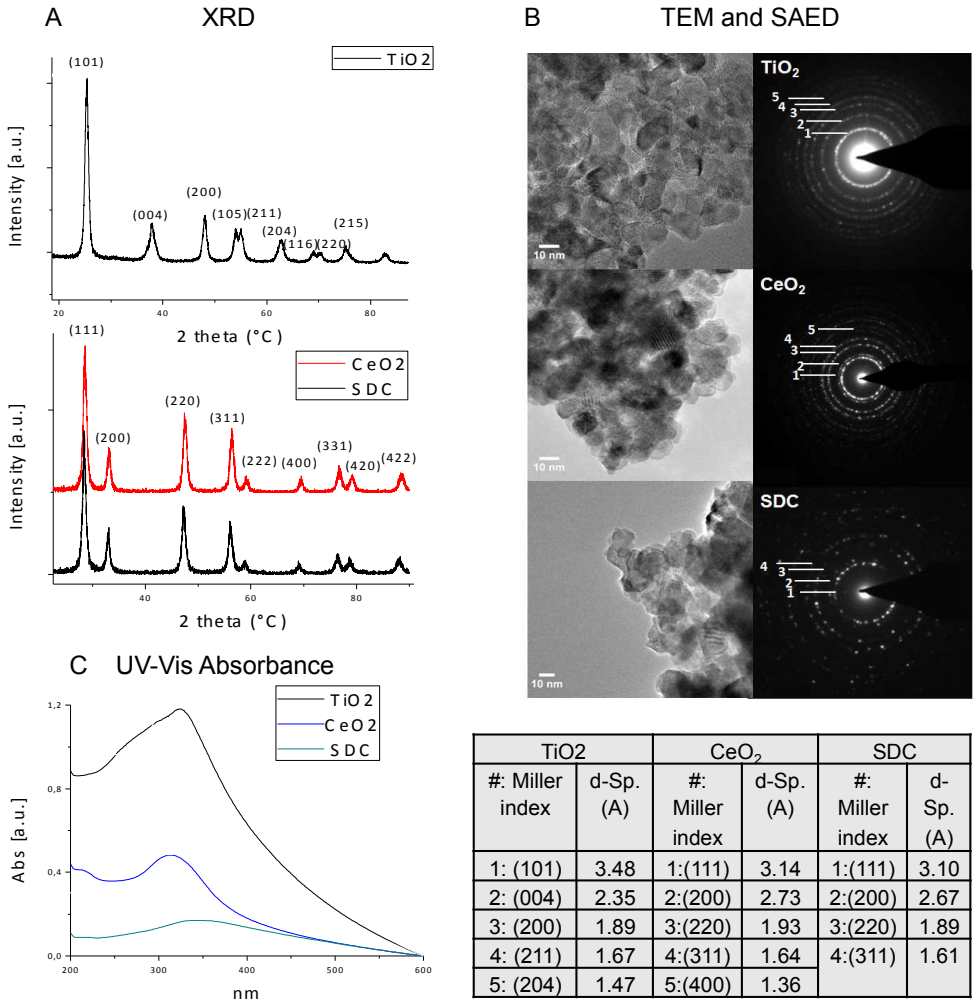

TiO2		CeO_2		SDC	
#: Miller index	d-Sp. (A)	#: Miller index	d-Sp. (A)	#: Miller index	d-Sp. (A)
1: (101)	3.48	1:(111)	3.14	1:(111)	3.10
2: (004)	2.35	2:(200)	2.73	2:(200)	2.67
3: (200)	1.89	3:(220)	1.93	3:(220)	1.89
4: (211)	1.67	4:(311)	1.64	4:(311)	1.61
5: (204)	1.47	5:(400)	1.36		

D Nanoparticles characterization summary

NPs	Physico-Chemical characterization			NPs dispersion in H_2O/RPMI+10% FBS		
	Crystal Structure	Size (nm)	SSA (m^2/g)	d (nm)	P.I.	Z pot. (mV)
TiO_2	Anatase	10	50	228±4/ 244±3	0.22±0.08/ 0.20±0.01	-35±1/ -7±2
CeO_2	Fluorite	10	57	230±20/ 266±5	0.23±0.02/ 0.21±0.02	-36±1/ -7±1
SDC	$Ce_{0.8}Sm_{0.2}O_2$ fluorite	13	47	470±40/ 450±7	0.28±0.03/ 0.15±0.03	-21±1/ 2±1

Figure 1. Physico-chemical characterization of TiO_2, CeO_2 and SDC nanoparticles. *(A) XRD diffraction patterns of TiO_2 CeO_2, and SDC nanoparticles. (B) TEM micrographs and SAED of NPs. Miller index and d-spacing values from SAED are reported on the table in panel D. (C) UV-Vis absorbance spectra for the NP suspensions. (D) Summary of NP powder and dispersion characteristics; SSA: specific surface area; NP dispersion characterization: mean hydrodynamic diameter (d), mean polydispersity index (P.I.) by DLS analysis (Cumulant analysis) and zeta potential of 200 µg/mL NP dispersions.*

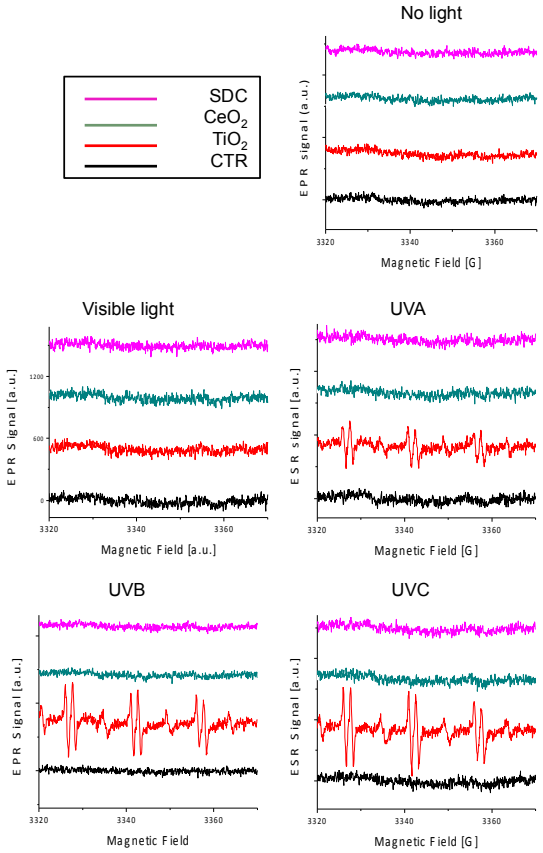

Figure 2. Nanoparticle photocatalytic activity. *EPR spectra of POBN-OH spin abduct signal produced by TiO_2, CeO_2 and SDC nanoparticles suspensions at 800 µg/mL. The signal produced by irradiated anatase is compatible with hydroxyl free radical, as shown by the hyperfine coupling constant values A_H = 15 G and A_N = 1.68 G.*

CeO_2 nanoparticles protect from UV-induced cell damage

TiO_2 nanoparticles exert protective effects on UV irradiated skin models[54-56], and one study reports that CeO_2 nanoparticles protect cells from the toxic effects of UV rays[25]. These results are complex to interpret, because both particles combine UV shielding properties with redox effects (antioxidant vs. pro-oxidant by TiO_2 vs. CeO_2 nanoparticles, respectively), and it is difficult to attribute the final effects to one or the other action. Indeed, the shielding and the redox effects are not easily separated, because *in vitro*, the cells most relevant for human exposure (e.g., skin fibroblasts or keratinocytes) grow in monolayers, and in the experimental conditions the powders are necessarily added as to form a sheet on top of cells. To separately evaluate the two effects, the UV-shielding should be removed or minimized.

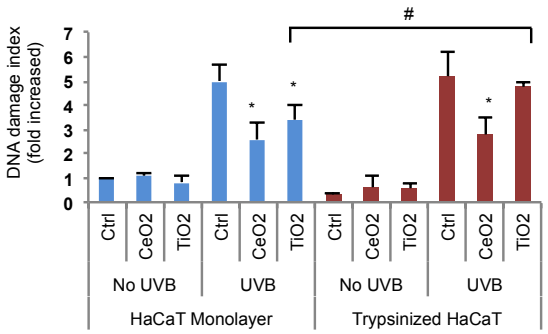

Figure 3. Differential protection of CeO_2 and TiO_2 nanoparticles in UVB-irradiated HaCaT monolayer vs. trypsinized HaCat*. DNA damage after irradiation with UVB. DNA damage was quantified by alkaline comet assay. All values are the mean of ≥ 3 independent experiments ± SD; *p < 0.05, #p < 0.05 (ANOVA). Significance of irradiated cells with respect to the UVB-irradiated cells group (*) and comparison between UVB-irradiated TiO_2 (#) are shown.*

To this purpose, we irradiated the human keratinocyte cells HaCat soon after detaching from the substrate by means of trypsin treatment; in this way keratinocytes become temporarily similar to cells growing in suspension (i.e., like blood cells); during irradiation, floating cells and powders were kept in gentle agitation to minimize UV shielding. Figure 3 shows the extent of DNA damage induced by UVB irradiation on HaCat forming monolayers, compared with the same HaCat irradiated while freely floating after trypsin treatment, in the presence/absence of CeO_2 or TiO_2 nanoparticles. It must be noticed that the extent of UVB-induced DNA damage is not influenced by the fact that cells adhere or float. As far as the effects of nanopowders are concerned, CeO_2 nanoparticles reduce UVB-induced DNA damage on keratinocytes in both conditions, whereas TiO_2 nanoparticles, which protect adherent cells, fail to significantly protect floating cells. This implies that the cytoprotective action of TiO_2 is due to their shielding effect, whereas CeO_2 nanoparticles essentially protect *via* their antioxidant properties.

To analyse the mechanisms through which CeO_2 nanoparticles exert their cytoprotective effect, we shifted to cells physiologically growing in suspension (i.e., blood cells instead of trypsinized keratinocytes) because some of the end-points (e.g., mutagenesis or cell cycle analyses) require long incubation times that would inevitably require re-adhesion of the trypsinized cells, *i.e.*, a poorly controllable condition. Our system of choice was thus Jurkat human T lymphocytes, because these cells have been thoroughly studied in

terms of cellular response to UV irradiation[57,58]. The experimental strategy adopted to analyse the modulation of UV-induced cytotoxicity on Jurkat cells is summarized in Figure 4. In a first round of experiments, we analysed UV-induced lesions by measuring the extent of DNA damage; the DNA damage response in terms of arrest of the cell division cycle; the extent of apoptosis; the rate of cell proliferation. The protocols for UV irradiation of cells were as follows: 3 mW/cm^2 of UVA for 60 minutes; 3 mW/cm^2 of UVB for 1 minute; and 2 mW/cm^2 of UVC for 0.5 minutes. The exposure times were chosen to get a similar (~ 50%) loss of cell viability at 24 h post-irradiation with UVB and UVC, whereas for UVA the exposure time was arbitrarily posed at 60 min to mimic a standard solar exposure. Cells were also irradiated with visible light (up to 1 h), in the presence and absence of the three nanopowders; in either case no toxic effects were observed. Figure 5 shows how the three types of nanoparticles modulate the acute toxicity of UVA, UVB and UVC on Jurkat cells in terms of DNA damage, cell cycle alterations, cell death by apoptosis, and inhibition of cell proliferation.

UVA irradiation per se was essentially non-toxic, whereas UVB and UVC produced DNA damage (Figure 5A) that caused cell cycle arrest in G2 phase (Figure 5B), inhibition of cell proliferation (Figure 5C), and cell death by apoptosis (Figure 5D). None of the powders were toxic without irradiation by any of the selected criteria. CeO_2 nanoparticles did not cause any toxicity by themselves, nor they increased the toxic effect of irradiation at any wavelength. In contrast, irradiated TiO_2 exerted strong toxic effects, especially evident upon UVA irradiation. This observation corroborates the EPR results, pointing to the fact that TiO_2 are the only particles able to produce the highly toxic hydroxyl radical as a result of the photocatalytic effect. The correlation between hydroxyl radical produced by irradiated anatase and cytotoxicity is shown in Figure 5E, where the amount of hydroxyl radical produced by TiO_2 for each wavelength (EPR analysis) is normalized to the actual time used to irradiate cells, and compared with the increment of toxicity by irradiated anatase.

In agreement with previous results[25,59], we showed that CeO_2 nanoparticles preserve the viability of UV-irradiated cells, abolishing apoptosis and maintaining high cellular proliferation rates. In addition to this, we showed that CeO_2 nanoparticles reduce UV-induced DNA lesions, to an extent (almost control level), that the DNA damage response is nearly abolished, since the arrest of their cell cycle is hardly detectable (see cell cycle profiles in Figure 5B). Overall, these results show that CeO_2 nanoparticles exert dramatic cell protection from UVB and UVC irradiation, strongly reducing cell toxicity measured by any criteria.

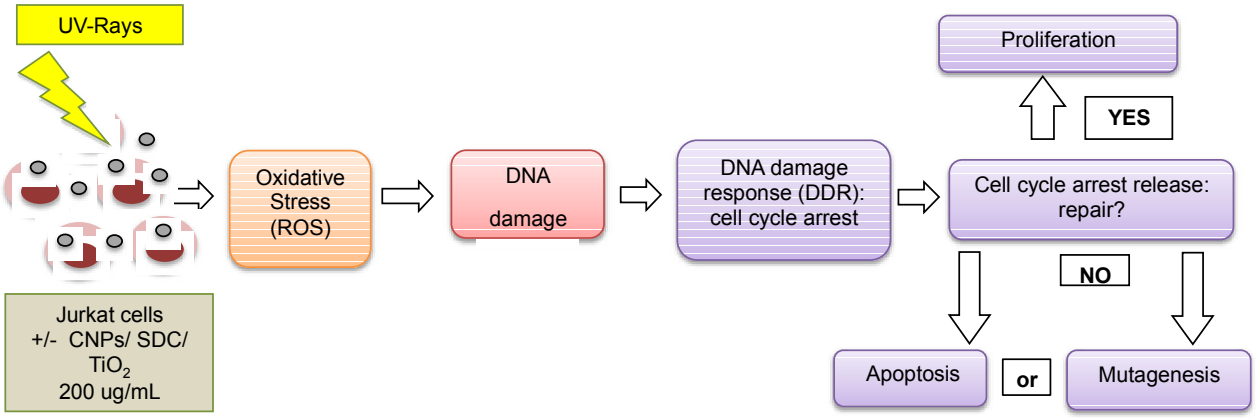

Figure 4. Experimental strategy. *A scheme of the experimental strategy adopted to analyse the modulation of UV-induced cytotoxicity on Jurkat cells± NPs (grey circles) is depicted, showing the set of cellular events in response to irradiation in chronological order; oxidative stress (orange box), DNA damage (red box) induced by irradiation, followed by the DNA damage response (purple box), that induce an arrest of the proliferative cycle and a tentative to repair the DNA damage. When the damage is repaired the cell cycle arrest is released, then cells enter mitosis and proliferate (green box), while in the presence of irreparable damage, cells undergo apoptosis or they proliferate in spite of the persistent damage, propagating mutations to the genome.*

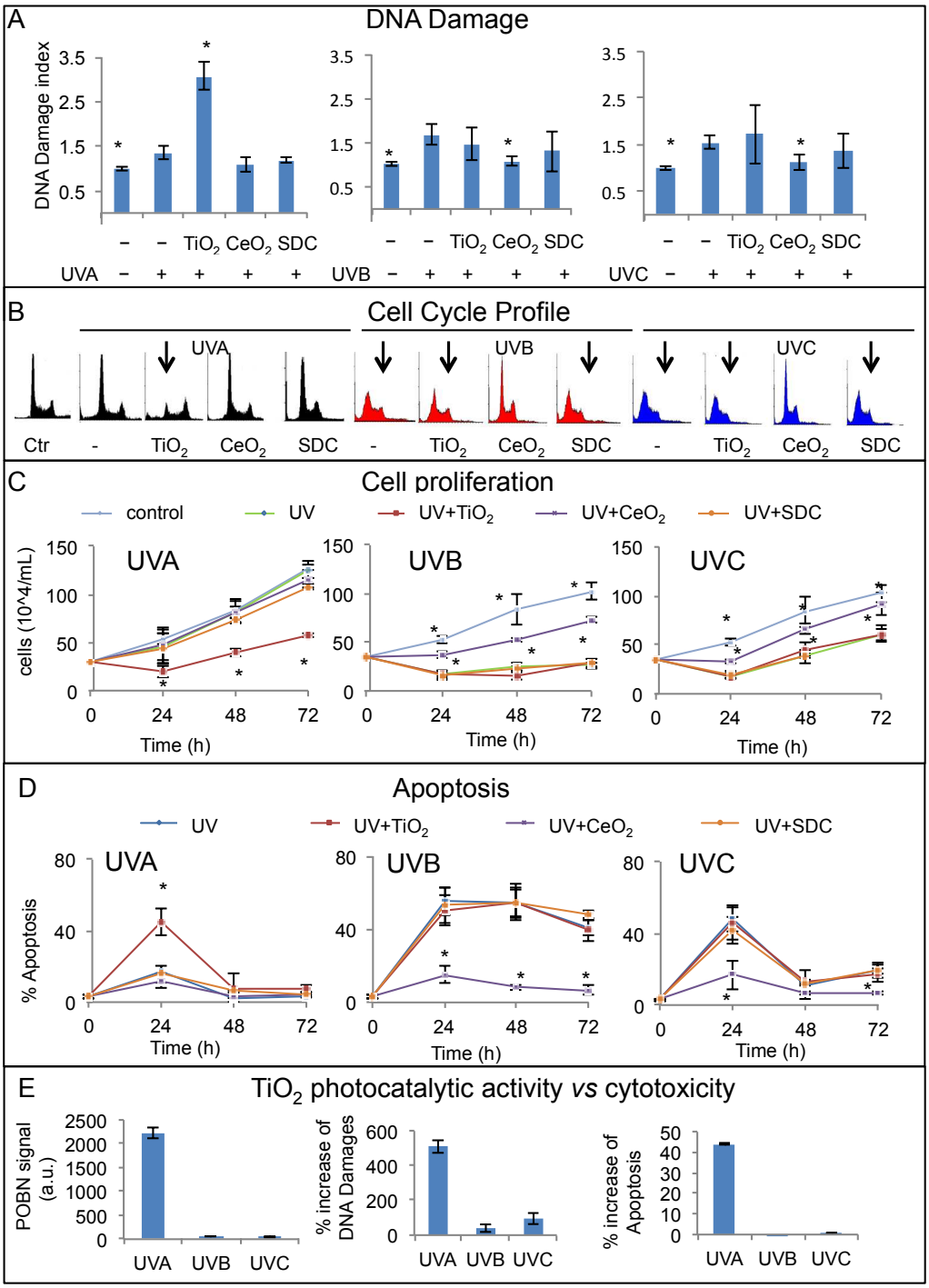

Figure 5. Modulation of cytotoxicity by nanoparticles. *(A) DNA damage index by comet assay 1 h after irradiation. (B) Cell cycle profiles 24 h post-irradiation: arrows indicate profile changes compared to control. Time course of cell proliferation (C) and apoptosis (D). For A-D: values are mean of ≥ 3 experiments ± SD; *p < 0.05 (ANOVA). Significance with respect to the UV-irradiated cells group is shown. (E) Quantification of UV-irradiated titania OH° radicals production normalized for cell irradiation time (60 min UVA, 1 min UVB and 30 s UVC) (left graph) and compared with the extra-toxicity induced by irradiated TiO_2.*

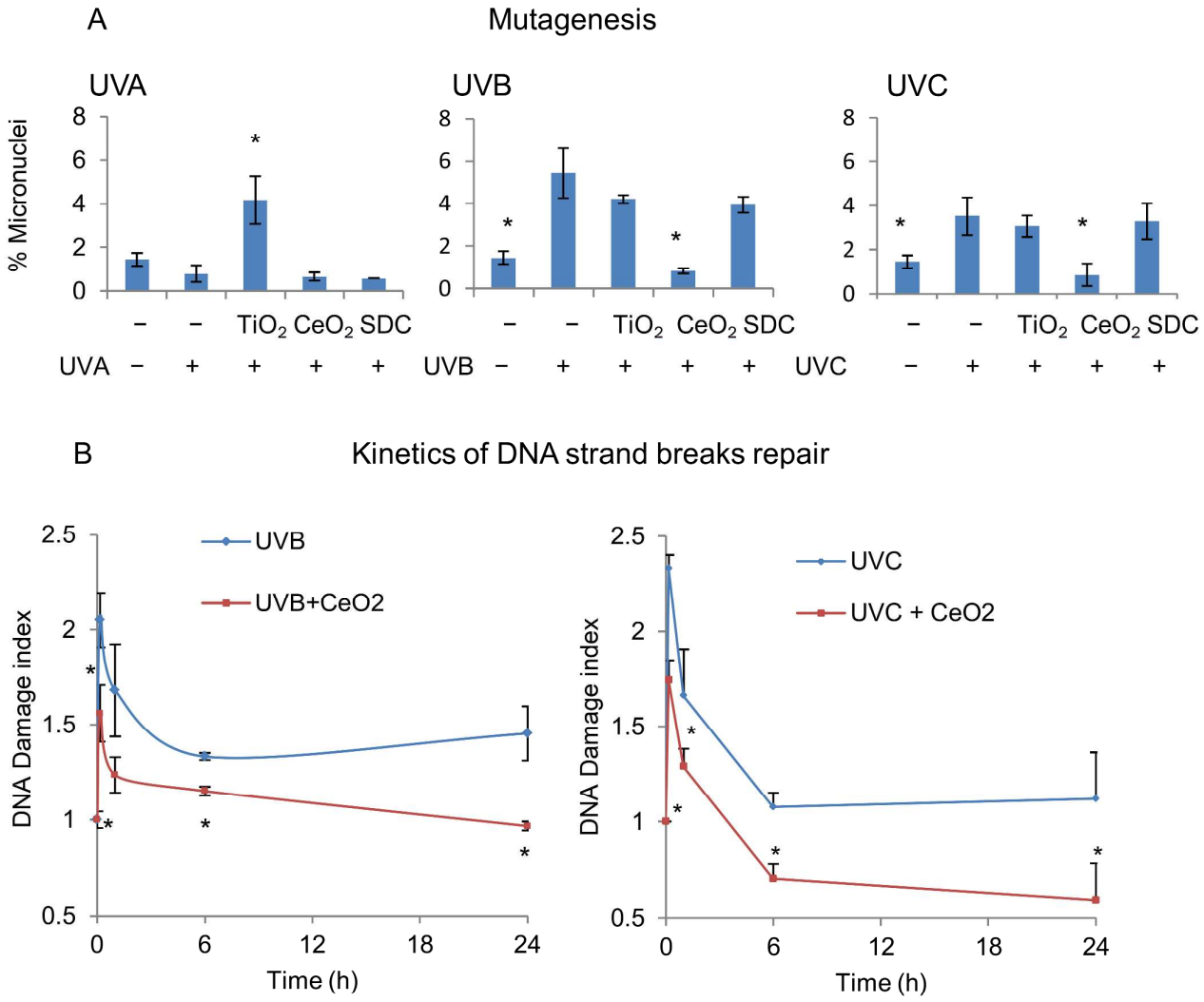

Figure 6: CeO_2 protects from UV-induced mutagenesis accelerating DNA repair. *Fraction of micronuclei among bi-nucleated cells. (B) Kinetics of DNA breaks after 1 min irradiation with UVB (left) and 30 sec irradiation with UVC (right). DNA damage was quantified by alkaline comet assay at the indicated time points; values are normalised to the control. All values are the mean of ≥ 3 independent experiment± SD; *p < 0.05 (ANOVA). Significance with respect to the UV-irradiated cells group is shown*

CeO_2 nanoparticles prevent UV-induced mutagenesis

The death of cells with damaged or mal-repaired DNA is a preferential solution as compared to the survival of damaged cells, the latter being a situation likely leading to mutations and eventually cancer. Therefore, the suicide of damaged cells by apoptosis eliminates potentially cancerous cells, being in fact the first barrier against carcinogenesis[60]. In this view, agents that decrease apoptosis, thereby preserving the mutated cells, do not exert a favourable effect to organism homeostasis; in such instances, decrease of apoptosis is accompanied by increased mutagenesis.

To understand whether, in our system, the decrease of apoptosis of irradiated cells by CeO_2 nanoparticles implied survival of mutated cells, we performed a mutagenesis analysis by evaluating the fraction of cells forming micronuclei, a test that encompasses a broad array of different types of chromosome mutations arising from mal-repaired DNA. Figure 6A shows that not only CeO_2 nanoparticles did not increase micronuclei formation upon UVB and UVC, but rather, mutagenesis was almost completely prevented.

The latter results provides the mechanistic bases to the reported ability of CeO_2 nanoparticles to exert anti-carcinogenic effects on UV-irradiated melanoma cells[61].

The type of DNA lesions induced by UVB and UVC (unlike those produced by ionizing radiations) are easily repairable[62]. In these instances, apoptosis and mutagenesis are more likely the consequence of insufficient, rather than wrong, repair (as instead occurs for ionizing radiations), and take place when the extent of the damage exceeds the number of enzymatic machineries available for DNA repair. Thus, the coexistence of strong anti-apoptotic and anti-mutagenic effects suggests that CeO_2 nanoparticles may accelerate the rate of DNA repair to reach completion before the onset of apoptosis or cell division. To test the rate of DNA repair we performed a time course of DNA breaks of cells irradiated by UVB in the presence/absence of CeO_2 nanoparticles. Figure 6B shows that in irradiated Jurkat cells sealing of DNA breaks begins soon after irradiation; after 24 h the amount of DNA breaks was reduced by ~50% with respect to the initial damage. In the presence of CeO_2 nanoparticles, repair was faster, and at 24 h completion was already reached. This result demonstrates that CeO_2 nanoparticles not only reduce UV-induced DNA damage, but also accelerate the rate of DNA repair. Base and nucleotide excision repair, the two major mechanisms involved in the repair of UV-irradiated DNA, include redox-sensitive enzymes where a cysteine-metal coordination group (a [4Fe-4S] cluster) is required for rapid detection of DNA damage through electrochemical gradients[63]; therefore it is conceivable that CeO_2 nanoparticles may reinforce the redox cycle of the enzymes involved, accelerating repair of the DNA double helix. Interestingly, it has been recently demonstrated that the anti-oxidant action of silymarin enhances the nucleotide excision repair (NER) mechanism in UV irradiated human fibroblasts. Therefore, it is conceivable that CeO_2 nanoparticles may reinforce the redox cycle of the enzymes involved, accelerating DNA repair[64].

Protection from UV-damage requires the Ce^{3+}/Ce^{4+} redox switch

To study the mechanism through which CeO_2 nanoparticles exert this effects, we explored if this is due to the antioxidant effect of CeO_2 nanoparticles. To do so, we compared the effects of CeO_2 nanoparticles with those of SDC, where the 3+ cerium ions are substituted by the fixed-valence 3+ Sm for all the experiments above described. Previous studies indicated that 20% doping completely abolished the redox switch and the biological effects[31] and therefore this degree of doping was chosen. As shown in Figure 5 and in Figure 6, Sm-doping prevented the cell-protective effects of CeO_2 nanoparticles for all parameters investigated, showing that the protective effect of CeO_2 nanoparticles requires the 3+/4+ valence switch, and is therefore related to their antioxidant ability.

To cross-check whether an antioxidant effect obtained by other means, i.e., by using the molecular radical scavenger N-acetyl-cysteine (NAC), would promote similar protective effects, we wanted to verify whether NAC would protect Jurkat cells from UVB and UVC-induced apoptosis and mutagenesis. Figure 7 shows that indeed NAC reduces the extent of UV-induced apoptosis (panel A) and mutagenesis (panel B), showing that this is an oxidation-related type of cell damage following UV irradiation, and confirming that CeO_2 nanoparticles protect via their antioxidant ability. Notably, the anti-apoptotic and anti-mutagenic effect of CeO_2 nanoparticles was more efficient than that exerted by NAC, suggesting that auto-regenerative CeO_2 nanoparticles protect from UV irradiation better that a stoichiometric molecular antioxidant.

To measure the direct antioxidant effects of CeO_2 nanoparticles in our system, we performed single cell analysis with dihydrorhodamine (DHR), an intracellular probe that detects a wide range of free radical species. Figure 7C shows that irradiation with UVA, UVB or UVC causes an increase of DHR signal. UVA induced ROS production to a similar extent as UVB or UVC, though they do not induce acute toxicity in our system; this suggests that either UVA-produced ROS are different, less toxic species compared with those produced by UVB or UVC, or that ROS are toxic only in the presence of direct DNA damage, an effect induced only by UVB and UVC. It is worth noting that Jurkat cells are devoid of the important UVA-specific chromophores such as melanin present in the skin, and that a fraction of melanin, in the form of pheomelanin, is responsible of UV-induced photocatalytic effect[65]. The lack of these UVA-specific chromophores may render Jurkat cells less subject to the acute toxicity that UVA may promote in skin cells.

The effects of the powders on UV-induced ROS production revealed a pro-oxidant effect of TiO_2 upon UVA irradiation, a strong antioxidant effect of CeO_2 nanoparticles, which reduced UVA-induced ROS production, and completely prevented ROS products generated by UVB and UVC, and a loss of protection by SDC, as expected.

Nanoscale

ARTICLE

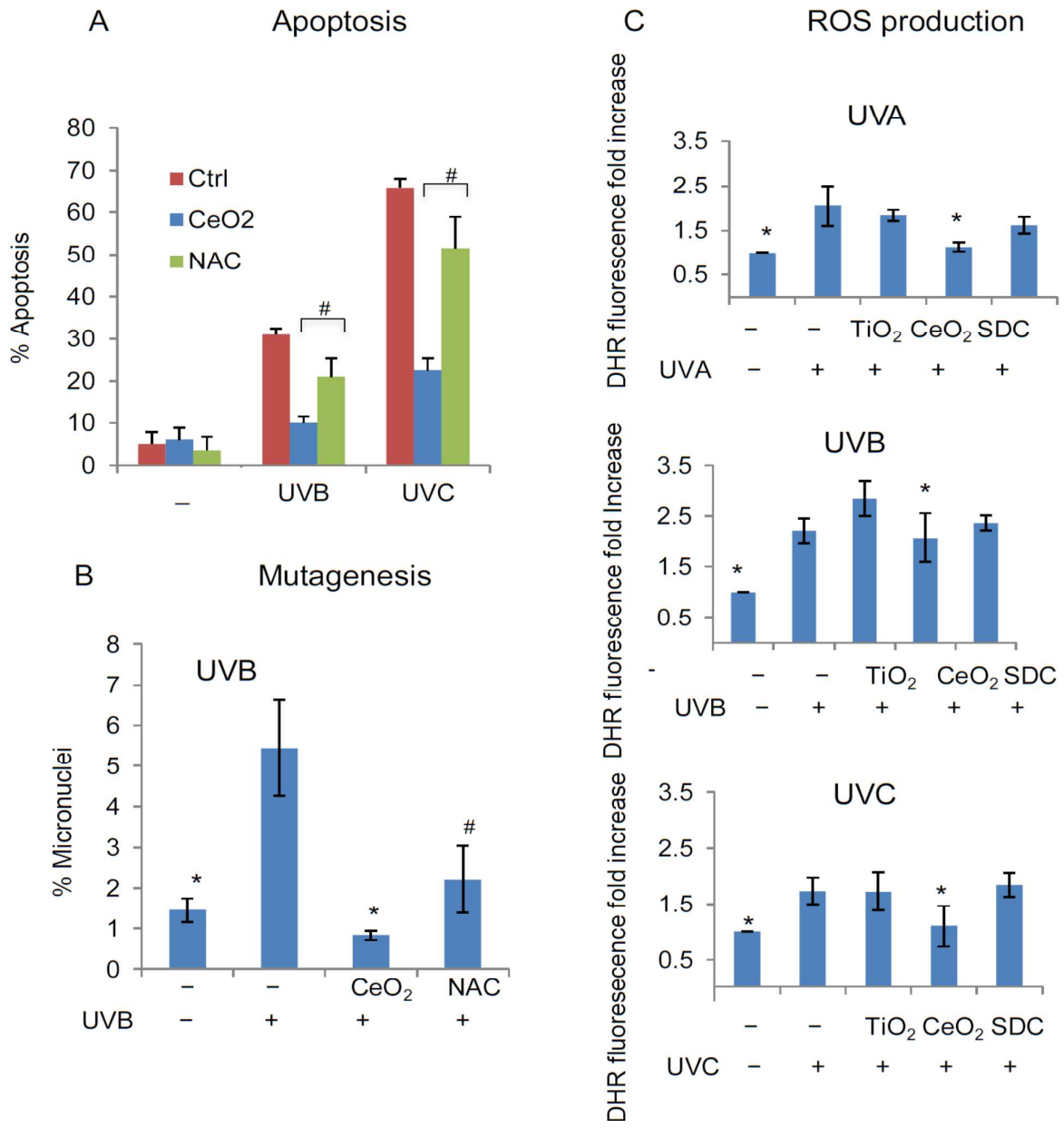

Figure 7. CeO_2 nanoparticles act as antioxidant in UV-irradiated Jurkat cells. *(A) Apoptosis in UVB and UVC irradiated cells pre-treated with CeO_2 nanoparticles (200 ug/mL for 24h) vs. NAC (1mM for 1h) for 1h. #p < 0.05 (ANOVA). Significance of the protection due to NAC pre-treatment with respect to CeO_2 pre-treatment is shown. (B) Micronuclei formation in UVB-irradiated cells pre-treated with CeO_2 vs. NAC, #p < 0.05 (ANOVA) and Vs without CeO_2 values, *p < 0.05. (C) DHR fluorescent signal detected by flow cytometry immediately after irradiation in cells ± NPs with UVA (60 min; 2 mW/cm^2), UVB (10 min; 3 mW/cm^2) and UVC (10 min; 3 mW/cm2). Values are the mean of ≥ 3 independent experiments ± SD; *p < 0.05 (ANOVA). Significance with respect to the UV-irradiated cells group is shown.*

CeO_2 nanoparticles protect cells from oxidative damage induced by UV-irradiated TiO_2

The antioxidant and cell protective effect of CeO_2 nanoparticles were then probed against the photocatalytic effect of TiO_2. In particular, the presence of CeO_2 nanoparticles with concentration ratios as low as 1:4 with respect to TiO_2 completely scavenged the hydroxyl radical produced by irradiated TiO_2, which became undetectable by EPR, suggesting that CeO_2 nanoparticles may act in competition with the POBN spin trap (Figure 8A). Similar results were obtained analyzing the cytotoxic effects: Figure 8B shows that CeO_2 nanoparticles dose-dependently protect from toxicity induced by UVA-irradiated TiO_2.

The scavenging of ROS produced by irradiated TiO_2 particles is a priority from the public health as well as from the commercial point of view, and the addition of molecular antioxidants to the TiO_2-based lotions has been attempted; however, the results were deceiving so far. To explore whether CeO_2 nanoparticles may be a better alternative to the molecular antioxidants, here we compared the scavenging effects of CeO_2 nanoparticles against ROS produced by irradiated TiO_2 nanoparticles, with that of efficient molecular antioxidants such as NAC and trolox, a soluble analog of vitamin E. Figure 8C shows that NAC and trolox did reduce the overall oxidative DCF signal of irradiated titania, but were significantly less efficient with respect to CeO_2 nanoparticles. This suggests that the stability of the antioxidant effect of CeO_2 nanoparticles, due to the auto-regenerative redox cycle, may overcome the problems of the stability of the molecular antioxidants.

The novel biological protective inter-particle cooperative effect, superimposed to the increase of the physical shielding of TiO_2/CeO_2 nanoparticles mixtures recently reported by Truffault et al.[30], discloses unexpected options to solve the problems related to the photo-toxicity of TiO_2.

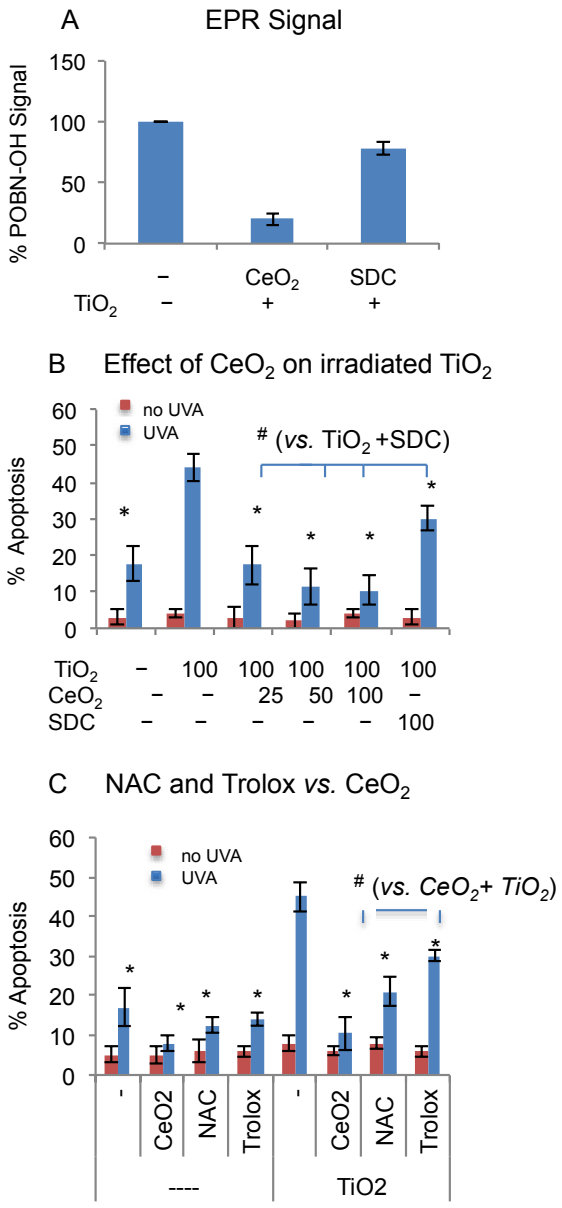

Figure 8. CeO_2 nanoparticles counteract the photocatalytic effects and cytoxicity of UVA-irradiated TiO_2. *(A) POBN-OH spin abduct produced by 800 µg/mL UVA irradiated TiO_2 ± 200 µg/mL CeO_2 or SDC. (B) Apoptosis 24 h after UVA irradiation of cells pre-treated with TiO_2 ± CeO_2 or SDC (25-200 µg/mL) for 24h. Values are the mean of ≥ 3 independent experiments ± SD; *,# $p < 0.05$ (ANOVA). Significance with respect to UVA-irradiated cells (*) or to the SDC+TiO_2 (mixture 1:1) (#) group is shown. (C) Apoptosis in UVA-irradiated cells pre-treated with CeO_2 (100 µg/mL for 24h), NAC (1mM for 1h)or Trolox (100uM for 30 min) ± TiO_2 (100 µg/mL for 24h) *,# $p < 0.05$ (ANOVA). Significance with respect to the UVA-irradiated cells (*) and to the CeO_2+TiO_2 (mixture 1:1) pre-treatment (#) is shown.*

Experimental

Synthesis and characterization of ceramic nanopowders. TiO_2, CeO_2 and 20% samarium doped ceria nanoparticles (SDC) were synthesized using wet-chemical procedures, as previously described[31,49-53]. TiO_2 nanoparticles were prepared by heating the dried TiO_2 precursor (Ti isopropoxide) to 450°C for 4 h. CeO_2 and SDC nanoparticles powders were prepared by heating the precursor to 450°C for 8 h. The temperatures were selected after characterizing the dried precursor using simultaneous thermogravimetric and differential thermal analysis (TG/DTA, Netzsch STA 409), performed in air flow (80 mL/min) from ambient temperature to 1200°C, with a 2°C/min heating rate. Phase and morphology of the materials were analyzed using X-ray diffraction (XRD, Philips X-Pert) analysis. Crystal structure was identified by comparison of XRD and selected area electron diffraction pattern (SAED) measurements; 2θ and d-spacing values were compared to references taken from the JCPDS data base (71-1166 for anatase, 75-0390 for CeO_2 fluorite structure and 75-0158 for 20% samarium doped cerium oxide). Nanoparticle dimensions were determined using transmission electron microscopy (TEM) analysis, performed at 300 keV electron beam energy by using a Titan G2 60-300 ST Cs-Image corrected microscope (FEI). Selected area electron diffraction (SAED) patterns were also acquired selecting an area of about 150 nm containing the sample nanoparticles. In addition, X-ray energy dispersive spectroscopy (EDS) and electron energy loss spectroscopy (EELS) analyses were performed to determine the elemental composition of samples. Specific surface area (BET analysis) measurements were performed treating the samples in helium flux at 300°C for 1 h using a Micromeritics Gemini V equipment.

Nanoparticle dispersions. A stock dispersion of CeO_2 and TiO_2 nanoparticles was prepared in deionized water at the concentration of 20 mg/mL. NPs were dispersed with ultrasounds (Branson Ultrasonic Corp., Danbury, CT, USA) at 20% amplitude for 5 minutes, and immediately diluted at the final concentration used for each experiments. Zeta potential and dynamic light scattering (DLS) of the NPs at the concentration of 200 µg/mL were measured immediately after sonication at 37°C in deionized H_2O (pH 7.4) or in RPMI medium + 10% fetal calf serum (FCS, to mimic cell culture environment), with a Malvern Zetasizer (Nano-ZS, Malvern Instruments, Worcestershire, UK). DLS experiments consisted of 15 runs per measurement and all experiments were carried out in triplicate. The mean ± standard deviation (SD) of the hydrodynamic diameter and the polydispersity index (P.I.) by cumulant analysis were calculated. Zeta potential experiments consisted of 100 runs per measurement and all experiments were carried out in triplicate. The mean of each triplicate measurement ± standard deviation (SD) is reported. Measurements in H_2O were made in general purpose mode; measurements in cell media were collected in monomodal mode due to the high conductivity of this sample (16 mS/cm). The Smoluchowski approximation was used to convert the electrophoretic mobility to zeta potential.

UV-Vis absorbance. Absorbance of NP suspensions in H_2O (pH 7.4) at the final concentration of 50 µg/mL was recorded in the 200-600 nm range using a UV-Vis spectrometer (Perkin Elmer Lambda 25 uv-vis spectrometer).

Electron paramagnetic resonance spectroscopy measurements.
A stock POBN solution was freshly prepared immediately before the experiments. NPs were sonicated and immediately dispersed in 0.1 M POBN solution at a final concentration of 800 µg/mL. Tests were performed without irradiation on POBN solution as a control and on POBN-NPs suspensions. The samples were irradiated at 25°C:
(i) for 20 minutes using a 150 W halogen light source at 10 W/cm^2, model KL1500 Electronic (Schott AG, Mainz, Germany).
(ii) for 10 minutes either with UVC at 2 mW/cm^2 (254 nm, Spectroline EF-140C/FE), or with UVA and UVB at 3 mW/cm^2 (365 nm and 312 nm respectively, Spectroline ENB-260C/FE).
During exposure to light, the 2-mL volumes of suspensions were equilibrated with oxygen at the atmospheric pressure and stirred vigorously to prevent aggregation of nanoparticles. To avoid overheating by light, the temperature of suspensions was stabilized at 25.0 ± 0.1°C using a Haake K10 bath vessel with a temperature control module Haake DC10 (Thermo Fisher Scientific GmbH, Karlsruhe, Germany).
After each illumination step, the suspension volumes of ~15 µL were drawn into thin-walled borosilicate glass capillaries (0.7 mm ID, 0.87 mm ED, Model CV7087-100, VitroCom Inc., Mountain Lakes, NJ, USA), sealed on both ends with a tube sealant, ChaSeal (Chase Scientific Glass Inc., Rockwood, TN, USA), and measured using an X-band ESR spectrometer, Model EleXsys 500, from Bruker Spectrospin, Karlsruhe, Germany, equipped with a super-high-Q cavity, Bruker Model ER 4122SHQE. The typical instrumental settings were: microwave frequency ~9.4 GHz, microwave power 0.65 mW, sweep width 120 G, modulation frequency 100 kHz,

modulation amplitude 0.5 G, receiver gain 60 dB, time constant 40.96 ms, conversion time 81.92 ms, and total scan time 167.8 s. Routinely, to improve the signal-to-noise ratio, two traces were accumulated for each ESR spectrum. Control ESR measurements were performed for all the POBN-nanoparticle suspensions prior to exposing them to light.

Cell cultures. Jurkat cells (human tumor T lymphocyte)[66], and HaCat cells (spontaneously transformed human keratinocyte), were grown at 37°C in RPMI 1640 medium (Jurkat) or in DMEM medium (HaCat cells), supplemented with 10% fetal calf serum (FCS), 100,000 units/L penicillin, 50 mg/L streptomycin, and 200 mM glutamine, in a humidified atmosphere of 5% CO_2 in air. All the experiments were performed on cells in the logarithmic phase of growth under condition of >96% of viability. In each experiment, Jurkat cells were kept at the concentration of 106 cells/mL, and HaCat cells confluence was kept at 80%.

Cell incubation with nanoparticles. NP suspensions were prepared at a final concentration of 200 µg/mL, sonicated as previously described[31] and immediately incubated with Jurkat cells or HaCat cells; experiments were performed after overnight pre-incubation with the nanoparticle suspensions.

Materials for cell treatments. Hoechst 33342, etoposide (VP16), propidium iodide (PI), ribonuclease enzyme (RNAse) and α-(4-Pyridyl-1-oxide)-N-tert-butylnitrone (POBN), N-acetyl-cysteine (NAC), 6-hydroxy-2,5,7,8-tetramethylchroman-2-carboxylic acid (trolox), normal melting point agarose, low melting point agarose, and all the other chemicals used in the comet assay technique were purchased from Sigma-Aldrich (St. Louis, MO). Dihydrorhodamine (DHR) was purchased from Molecular Probes (Eugene, OR). Stock solutions: Hoechst 33342 (10 mg/mL), RNAse (20 mg/mL) and POBN 0.5 M were dissolved in distilled water; DHR (10 mM) was dissolved in dimethyl sulfoxide (DMSO); PI (5 mg/mL) was dissolved in distilled water.

Cell irradiation. Unless otherwise indicated, cells were placed in 24-well culture plates in complete medium without phenol red, and irradiated at room temperature with:

(i) visible light at 10 W/cm^2, using a 150 W halogen light source at Model KL1500 Electronic (Schott AG, Mainz, Germany) for 60 minutes.

(ii) UVA (365 nm, Spectroline lamp model ENB-260C/FE) at 3 mW/cm^2, for three times 20 minutes each, separated by two intervals of 10 minutes each, during which the cells were kept at 37°C and 5% CO_2;

(iii) UVB (312 nm, Spectroline lamp model ENB-260C/FE) single exposure at 3 mW/cm^2 for 1 minute.

(iiii) UVC (254 nm, Spectroline lamp model EF-140C/FE) single exposure at 2 mW/cm^2 for 30 seconds.

During irradiation of trypsinized or suspended cells, the cell/nanopowder suspensions were kept in constant gentle agitation.

Cell treatments with molecular antioxidants. Prior to the irradiation Jurkat cells were pre-incubated with NAC at the final concentration of 10 mM for 1h or with Trolox at the final concentration of 100 µM for 30 minutes.

Analysis of cell proliferation. The rate of cell proliferation was assessed by evaluating cell concentration at increasing time points after irradiation using a Burker counting chamber; values are given as number of cell/mL.

Evaluation of apoptosis. Apoptosis was evaluated quantifying the fraction of apoptotic nuclei by fluorescence microscopy after DNA staining with the cell-permeable specific dye Hoechst 33342, directly added to the cell culture at the final concentration of 10 µg/mL[67]. To evaluate the eventual presence of necrotic cells, cells were also stained with PI at a final concentration of 5 µg/mL. The fraction of apoptotic nuclei among the total cell population was calculated by counting at the fluorescence microscope at least 300 cells in at least three independent randomly selected microscopic fields. In addition, apoptosis was estimated by quantifying the sub-G1 apoptotic peak in the cell cycle profile; the two methods gave similar values.

Cell cycle analysis. Cells were washed with PBS and fixed overnight in ethanol 70% at 20°C, treated with RNAse at 200 µg/mL, stained with PI at the final concentration of 50 µg/mL and finally analyzed by FACSCalibur flow cytometer. 20,000 cells were analyzed for each sample. Data were analyzed with WinMdi 2.9 software.

DNA damage analysis by alkaline Comet assay.

Alkaline Comet assay is a single-cell gel electrophoresis method that allows detecting single and double strand DNA breaks[68]. One hour after irradiation (unless otherwise stated) cells were suspended in 0.5% low melting point agarose then pipetted onto a frosted glass microscope slide pre-coated with a layer of 0.2% normal melting point agarose. Slides were incubated in an alkaline lysis solution for 40 min (Jurkat cells) or for 1 h (HaCat cells). After cell lysis, slides

were rinsed with electrophoresis buffer to allow DNA unwinding. Electrophoresis was conducted with the Subcell GT System/15x25 cm equipped with Power Pack 300 (Bio Rad Laboratories Inc, Hercules, CA, USA) at 20 V, 350 mA for 18 min (Jurkat cells) or 30 min (HaCat cells). Subsequently, slides were gently washed in neutralization buffer solution for 5 min, and then dehydrated with ethanol series, and dried at room temperature. One hundred cells on each slide were scored using a fluorescence microscope; the extent of genetic damage was evaluated by visual scoring provided in arbitrary units[69].

Detection and quantification of intracellular ROS. Reactive oxygen species (ROS) were measured by dihydrorhodamine (DHR), a probe that is internalized in cells and fluoresces only when oxidized to rhodamine[70], allowing quantitative assessment of intracellular ROS. Before the measurement cells were irradiated with UVA (60 minutes, 3 mW/cm^2), UVB (10 minutes, 3 mW/cm^2) or UVC (10 minutes, 2 mW/cm^2). Immediately after the irradiation DHR was added directly to the cell samples to a final concentration of 2 µM and incubated at 37 °C in the dark for 20 min; then cells were analyzed by FACSCalibur flow cytometer; 10,000 cells were analyzed for each sample. Data were analyzed with WinMdi 2.9 software; the mean values were used for tables and graphs.

Mutagenesis analysis via the micronuclei assay. The micronuclei test is a broad-spectrum mutagenesis test[71]. Micronuclei are small nuclear bodies arising from improper chromosome separation at mitosis as a consequence of mal-repaired DNA damage. Evaluation of the fraction of micronuclei among cells undergoing mitosis is a measure of early mutagenesis after genotoxic treatments. After irradiation, cytochalasin B (3 µg/mL; Sigma) was added to the cells to prevent cell division without inhibiting mitosis: after 24 h, the resulting bi-nucleated cells label those that underwent mitosis. Then the medium was removed, the cells were rinsed with PBS, treated with hypotonic solution (KCl 0.075 M) for 3 min and then fixed with Carnoy fixative (methanol/acetic acid, 20:1) for 8 min and then stained with Hoechst 33342. 500 bi-nucleated cells were scored under a fluorescent microscope; the values given in the graphs represent the number of micronuclei per 500 bi-nucleated cells.

Statistical analysis. Each experiment was repeated ≥ 3 times. Data are presented as means ± SD. Statistical evaluation was conducted by a one-way ANOVA, followed by Tukey's Multiple Comparison Test (Homogeneous Variances) using the software SPSS 16.0. Statistical significance was set at $p < 0.05$.

Conclusions

We have demonstrated that the extra-shielding properties of irradiated TiO_2 nanoparticles exert highly damaging effects via production of the hydroxyl radicals, whereas CeO_2 nanoparticles allow striking cell and genetic protection against UV-induced damage. The phototoxic action of UVA and UVB-irradiated TiO_2 nanoparticles is highly relevant to the impact of exposure of human skin to ultraviolet light, because UVA and UVB reach the Earth surface, and TiO_2 is the main active component of widely used sun shield lotions. Considering that modern life habits would hardly abandon the practice of direct exposure to sunlight, an efficient technological solution to the adverse effects of UV-irradiated TiO_2 nanoparticles is very much needed. Therefore, CeO_2 nanoparticles seem to be the ideal candidates to overcome the problems connected with the photocatalytic effect of TiO_2 nanoparticles. Sunscreen lotions are applied above the stratum corneum, the tough cutaneous barrier that is impermeable to nanoparticles; therefore, the photocatalytic effect of TiO_2 nanoparticles-based lotions develops above the skin surface, being rather harmless to intact epidermis[19,72]. The health hazard arises when the stratum corneum becomes leaky in bruised or erythematous skin, a frequent consequence of sunburns, allowing penetration of nanoparticles that thus come into physical contact with the living cells in the deep underlying derma[21,72]. This is a scenario rather similar to our experimental system, where nanopowders and cells are mixed together: in such instances, the cell damaging or protective effects of nanoparticles becomes highly relevant. This reflects many recent studies reporting that TiO_2 protect from UVA irradiation ex vivo skin specimen and skin models[54-56], but not cultured keratinocytes or dermal fibroblasts[13-18], where the nanoparticles are in contact with the living cells. This is specific for UVA[73], as confirmed by our experiment with UVB-irradiated HaCat cells, where TiO_2 nanoparticles exert a protective effect due to their shielding power.

Strategies to bypass the risks of TiO_2 nanoparticles photocatalytic effect have been attempted, such as the deactivation of the photocatalytic effect of the nanoparticle surface by molecular capping[23] or inert oxides coating[23], with unsatisfactory outcomes[21].

Recently an alternative strategy has been proposed, consisting in the inclusion of antioxidants in TiO_2-based formulations[22-24,74]. The use of nano-antioxidant, such as fullerene[24] and silver nanoparticles,[75] has been reported to scavenge the oxidative stress induced by UV irradiation, exerting cell protection in keratinocytes irradiated in the presence of TiO_2[24]. Our study suggests that CeO_2 nanoparticles, which combine UV-shielding with potent antioxidant action, may be a successful adjuvant in TiO_2-based lotions formulae because of their impressive protection against damage induced directly by UV in general, and by the photocatalytic effect of irradiated TiO_2 nanoparticles in particular. Additional bonus that CeO_2 nanoparticles would provide include their potent anti-inflammatory properties[32,36], which would contrast UV-induced local (erythema) and systemic pro-inflammatory effects; the small size of CeO_2 nanoparticles (< 10 nm), which would guarantee transparency of the sunscreen lotions, a key asset from the commercial point of view; and the high UV refracting ability, which would contribute to the overall shielding efficiency of TiO_2 nanoparticles-based sun creams. Therefore, CeO_2 nanoparticles possess the requirements to be a breakthrough in solar shield technology, and research aimed at investigating their efficacy and safety in specific applicative studies should be considered as a priority.

Acknowledgements

F.C. and M.D.N. are recipient of fellowships from the PhD school in Materials for Health, Energy and Environment, Università di Roma Tor Vergata. We wish to thank Dr. Vittoria Maresca, Ospedale S. Gallicano (Roma, Italy), and Prof. Giampiero Gualandi, Università La Tuscia (Viterbo, Italy) for invaluable support. Thanks are due to Prof. Francesco Stellacci and Dr. Marta Mameli, École Polytechnique Fédéral de Lausanne (EPFL, Lausanne, Switzerland) for invaluable discussions and support. We thank Dr. Dalaver H. Anjum, King Abdullah University of Science and Technology (KAUST, Thuwal, Saudi Arabia) for assistance in TEM observations, Mss. Marianeve Polimeno and Ms. Monica Maio (Dipartimento di Biologia, Università di Roma Tor Vergata) for the experiments with HaCat cells.

Notes and references

1 H. Merwald, G. Klosner, C. Kokesch, M. Der-Petrossian, H. Hönigsmann, and F. Trautinger, *J Photochem Photobiol B: Biol*, 2005, **79**, 197.
2 F. E. L. Ghissassi, R. Baan, K. Straif, Y. Secretan, V. Bouvard, V L. Benbrahim-Tallaa, N. Guha, C. Freeman, L. Galichet and V. Cogliano, *Lancet Oncol,* 2009, **10**, 751.
3 G. T. Wondrak, M. K. Jacobson and E. Jacobson, *Photochem Photobiol Sci,* 2006, **5**, 215.
4 L. F. Z. Batista, B. Kaina, R. Meneghini and C. F. M. Menck, *Mutat Res,* 2009, **681**, 197.
5 A. T. Black, M. K. Gordon, D. E. Heck, M. A. Gallo, D. L. Laskin and J. D. Laskin, *Biochem Pharmacol,* 2011, **81**, 873.
6 G. J. Clydesdale, G. W. Dandie and H. K. Muller, *Immunol Cell Biol,* 2011, ***79***, 547.
7 A. Rampaul, I. P. Parking and L. P. Cramer, *J Photochem Photobiol A: Chem,* 2007, **191**, 138.
8 Z. A. Lewicka, A. F. Benedetto, D. N. Benoit, W. W. Yu, J. D. Fortner and V. L. Colvin, *J Nanopart Res,* 2011, **13**, 3607.
9 Z. Wang, M. Wanhong, C. Chuncheng, H. Ji and J. Zhao, J., *Chem Eng J,* 2011, **170**, 353.
10 T. Uchino, H. Tokunaga, M. Ando and H. Utsumi, *Toxicol in Vitro*, 2002, **16**, 629.
11 M. Nag, D. Guin, P. Basac and S. V. Manorama, *Mater Res Bull*, 2008, **43**, 3270.
12 K. Pierzchała, M. Lekka, A. Magrez, A. J. Kulik, L. Forro and A. Sienkiewicz, *Nanotoxicology*, 2012, **6**, 813.
13 C. Xue, J. Wu, F. Lan, W. Liu, X. Yang, F. Zeng, and H. Xu, *J Nanosci Nanotechnol*, 2010, **10**, 8500.
14 H. O. Park, M. Yu, S. K. Kang, S. I. Yang and Y-J. Kim, (2011) *Mol Cell Toxicol*, 2011, **7**, 67.
15 A. Jaeger, D. G. Weiss, L. Jonas and R. Kriehuber, *Toxicology*, 2012, ***296***, 27.
16 J. J. Yin, J. Liu, M. Ehrenshaft, J. E. Roberts, P. P. Fu, R. P. Mason and B. Zhao, *Toxicol Appl Pharmacol*, 2012, **263**, 81.
17 I. Fenoglio, J. Ponti, E. Alloa, M. Ghiazza, I. Corazzari, R. Capomaccio, D. Rembges, S. Oliaro-Bosso, and F. Rossi, *Nanoscale*, 2013, **21**, 6567.
18 F. Rancan, B. Nazemi, S. Rautenberg, M. Ryll, S. Hadam, Q. Gao, S. Hackbarth, S. F. Haag, C. Graf, E. Rühl, U. Blume-Peytavi, J. Lademann, A. Vogt and M. C. Meinke, *Skin Res Technol*, 2014, **20**, 182.
19 M. Skocaj, M. Filipic, J. Petrovic and S. Novak, S. *Radiol Oncol*, 2011, **45**, 227.
20 B. Vileno, M. Lekka, A. Sienkiewicz, S. Jeney, G. Stoessel, J. Lekki, L. Forró and Z. Stachura, *Environ Sci Technol*, 2007, **41**, 5149.
21 E. Gilbert, F. Pirot, V. Bertholle, L. Roussel, F. Falson and F. Padois, *Int J Cosmet Sci,* 2013, **35**, 208.
22 C. Xue, W. Liu, J. Wu, X. Yang and H. Xu, *Toxicol In* Vitro, 2011, **25**, 110.
23 T. G. Smijs and S. Pavel, S., *Nanotechnol Sci Appl*, 2011, **4**, 95;
24 S. Kato, H. Aoshima, Y. Saitoh and N. Miwa, *J Nanosci Nanotechnol*, 2014, **14**, 3285.
25 N. M. Zholobak, V. K. Ivanov, A. B. Shcherbakov, A. S. Shaporev, O. S. Polezhaeva, A. Y. Baranchikov, Y. N. Spivak and Y. D. Tretyakov, *J Photochem Photobiol B: Biol*, 2011, **102**, 32.
26 T. Herrling, M. Seifert and K. Jung, *SOFW-Journal 139*, 10-15.
27 S. Yabe, T. Sato, J Solid State Chem, 2003, **171**, 7.
28 L. Truffault, M-T. Ta, T. Devers, K. Konstantinov, V. Harel, C. Simmonard, C. Andreazza, I. P. Nevirkovets, A. Pineau, O. Veron, J-P. Blondeau, Mater Res Bull, 2010, **45**, 527.
29 R. Li, S. Yabe, M. Yamashita, S. Momose, S. Yoshida, S. Yin, T. Sato, Mater Chem Phys, 2002, **75**, 39.
30 L. Truffault, B. Winton, B. Choquenet, C. Andreazza, C. Simmonard, T. Devers, K. Konstantinov, C. Couteau, L. J.M. Coiffard, *Mater Lett*, 2012, **68**, 357.

31 I. Celardo, M. De Nicola, C. Mandoli, J. Z. Pedersen, E. Traversa and L. Ghibelli, *ACS Nano*, 2011, **5**, 4537.
32 I. Celardo, J. Z. Pedersen, E. Traversa and L. Ghibelli, *Nanoscale*, 2011, **3**, 1411.
33 S. Das, J. M. Dowding2, K. E. Klump, J. F. McGinnis, W. Self, S. Seal, Future Medicine, 2013, **8**, 1483.
34 S. Das , S. Chigurupati , J. Dowding , P. Munusamy , D. R. Baer , J. F. McGinnis, M. P. Mattson , W. Self , S. Seal, *MRS Bullettin*, 2014, **39**, 976.
35 A. Karakoti, S. Singh, J. M. Dowding, S. Seal, W. T. Self, *Chem Soc Rev*, 2010, **39**, 4422.
36 I. Celardo, E. Traversa and L. Ghibelli, *J Exper Therap Oncol*, 2011, **9**, 47.
37 E. G. Heckert, A. S. Karakoti, S. Seal and W. T. Self, *Biomaterials*, 2008, **29**, 2705.
38 T. Pirmohamed, J. M. Dowding, S. Singh, B. Wasserman, E. Heckert, A. S. Karakoti, J. E. King, S. Seal and W. T. Self, *Chem Commun*, 2010, **28**, 2736.
39 J. Colon, N. Hsieh, A. Ferguson, P. Kupelian, S. Seal, D. W. Jenkins and C. H. Baker, *Nanomedicine*, 2010, **6**, 698.
40 M. Das, S. N. Bhargava, J. F. Kang, L. M. Riedel, S. Seal, and J. J. Hickman, *Biomaterials*, 2007, **28**, 1918.
41 Y. Y. Tsai, J. Oca-Cossio, K. Agering, N. E. Simpson, M. A. Atkinson, I. Constantinidis and W. Sigmund, *Nanomedicine*, 2007, ***2***, 325.
42 J. Chen, S. Patil, S. Seal and J. F. McGinnis, *Nat Nanotechnol*, 2006, **1**, 152.
43 J. Colon, L. Herrera, S. Patil, P. Kupelian, S. Seal, D. W. Jenkins, C. W and C. H. Baker, *Nanomedicine*, 2009, **5**, 225.
44 D. González-Flores, M. De Nicola, E. Bruni, F. Caputo, A. B. Rodríguez, J. Pariente and L. Ghibelli, *Mol Cell Biochem*, 2014, **397**, 245.
45 F. Caputo, M. De Nicola and L. Ghibelli, *Biochem Pharmacol,* **92**, 112.
46 C. Walkey, S. Das, S. Seal, J. Erlichman, K. Heckman, L. Ghibelli, E. Traversa, J. F. McGinnis and W. T. Self, *Environ Sci: Nano*, 2015, **2**, 33.
47 M. Sack, L. Alili, E. Karaman, S. Das, A. Gupta, S. Seal, P. Brenneisen, *Mol Cancer Ther*, 2014, **13**, 1740.
48 L. Alili, M. Sack, A. S. Karakoti, S. Teuber, K. Puschmann, S. M. Hirst, C. M. Reilly, K. Zanger, W. Stahl, S. Das, S. Seal, P. Brenneisen, *Biomaterials*, 2011, **32**, 2918.
49 E. Traversa, M. L. Di Vona, S. Licoccia, M. Sacerdoti, M. C. Carotta, L. Crema and G. Martinelli, *J. Sol-Gel Sci Technol*, 2001, **22**, 167.
50 S. Licoccia and E. Traversa, *J Power Sources*, 2006, **159**, 12.
51 C. Mandoli, F. Pagliari, S. Pagliari, G. Forte, P. Di Nardo, S. Licoccia and E. Traversa, *Adv Func Mat*, 2010, **20**, 1617.
52 V. Esposito and E. Traversa, *JACS*, 2008, **91**, 1037.
53 F. Pagliari, C. Mandoli, G. Forte, E. Magnani, S. Pagliari, G. Nardone, S. Licoccia, M. Minieri, P. and E. Traversa, *ACS Nano*, 2012, **6**, 3767.
54 C. Augustin, C., Collombel and O. Damour, *Photochem Photobiol*, 1997, **66**, 853.
55 S. Boisnic, M. C. Branchet-Gumila, C. Merial-Kieny and T. Nocera, *Skin Pharmacol Physiol*, 2005, **18**, 201.
56 R. Haywood, A. Volkov, C. Andrady and R. Sayer, *Free Radic Res*, 2012, **46**, 265.
57 A. B. Scoltock and J. A. Cidlowski, *Exp Cell Res*, 2004, **297**, 212;
58 Y. Zhang, J. S. Wang, L. L. Chen, Y. Zhang, X. K. Cheng, F. Y. Heng, N. H. Wu and Y. F. Shen, *J Biol Chem*, 2004, **279**, 42545.
59 N.M. Zholobak, A.B. Shcherbakov, A.S. Bogorad-Kobelska, O. S. Ivanova, A.Y. Baranchikov, N. Y. Spivak, V. K. Ivanov, *J Photochem Photobiol, B*, 2014, **130**, 102.
60 F. Caputo, R. Vegliante and L. Ghibelli, *Biochem Pharmacol*, 2012, **84**, 1292.
61 L. Alili, M. Sack, C. von Montfort, S. Giri, S. Das, K. S. Carroll, K. Zanger, S. Seal, P. Brenneisen, *Antioxidants & Redox Signaling*, 2013, **19**, 765.
62 R. P. Sinha and D. P. Häder, *Photochem Photobiol*, 2002, **1**, 225.
63 O. A. Lukianova and S. S. David, *Curr Opin Chem Biol*, 2005, **9**, 145.
64 S. K. Katiyar, S. K. Mantena and S. M. Meeran, *PLoS One*, 2011, ***6***, e21410.
65 J. M. Wood and K. U. Schallreuter, *J Invest Dermatol*, 2006, **126**, 13.
66 U. Schneider, H. U. Schwenk and G. Bornkamm, *Int J Cancer*, 1977, **19**, 621.
67 L. Ghibelli, C. Nosseri, S. Coppola, V. Maresca and L. Dini, L., *Exp Cell Res,* 1995, **221**, 270.
68 A. Giovanetti, E. Basso and T. Deshpande, *Int J Rad Biol,* 2008*,* **84**, 227.
69 A. R. Collins, *Mol Biotechnol*, 2004, **26**, 249.
70 F. Radogna, L. Paternoster, M. De Nicola, C. Cerella, S. Ammendola, A. Bedini, G. Tarzia, K. Aquilano, M. Ciriolo and L. Ghibelli, *Toxicol Appl Pharmacol*, 2009, **239**, 37.
71 P. I. Countryman and J. A. Heddle, *Mutat Res*, 1976, **41**, 321.
72 M. D. Newman, M. Stotland and J. I. Ellis, *J Am Acad Dermatol*, 2009, **61**, 685.
73 H. Ma, A. Brennan and S. A. Diamond, *Environ Toxicol Chem*, 2012, **31**, 2099.
74 M. E. Carlotti, E. Ugazio, L. Gastaldi, S. Sapino, D. Vione, I. Fenoglio and B. Fubini, *J Photochem Photobiol B*, 2009, **96**, 130.
75 S. Arora, N. Tyagi, A. Bhardwaj, L. Rusu, R. Palanki, K. Vig, S. R. Singh, A. P. Singh, S. Palanki, M. E. Miller, J. E. Carter and S. Singh, *Nanomedicine*, 2015, DOI: 10.1016/j.nano.2015.02.024.